International Journal of Mechanical, Industrial and Aerospace Sciences
ISSN: 2517-9950
Vol:10, No:8, 2016

Tool Condition Monitoring of Ceramic Inserted Tools in High Speed Machining through Image Processing

Javier A. Dominguez Caballero, Graeme A. Manson, Matthew B. Marshall

***Abstract*—**Cutting tools with ceramic inserts are often used in the process of machining many types of superalloy, mainly due to their high strength and thermal resistance. Nevertheless, during the cutting process, the plastic flow wear generated in these inserts enhances and propagates cracks due to high temperature and high mechanical stress. This leads to a very variable failure of the cutting tool. This article explores the relationship between the continuous wear that ceramic SiAlON (solid solutions based on the Si3N4 structure) inserts experience during a high-speed machining process and the evolution of sparks created during the same process. These sparks were analysed through pictures of the cutting process recorded using an SLR camera. Features relating to the intensity and area of the cutting sparks were extracted from the individual pictures using image processing techniques. These features were then related to the ceramic insert's crater wear area.

***Keywords*—**Ceramic cutting tools, high speed machining, image processing, tool condition monitoring, tool wear.

I. Introduction

IN a machining process where great productivity is required, it is important to obtain a high chip removal rate. There are a number of different parameters associated with the machining process, such as feed, depth of cut and cutting speed, which could be altered to obtain a high chip removal rate. The most common choice for increasing removal rate is to increase the cutting speed, given that increasing the other two parameters could result in a wider chip cross-section, and hence higher cutting forces [1]-[3]. However, when the cutting speed is increased, this results in higher stresses and higher temperatures in the cutting area, therefore demanding greater strength and thermal resistance from the cutting tool. Traditional cemented tungsten carbides have good performance up to around 800 °C however, at higher temperatures, their strength decreases dramatically. By contrast, ceramic cutting tools show good performance up to 1200 °C [2]. These ceramic materials are known to produce higher metal removal rates than carbide materials when milling heat resistant super alloys, given that the operating speeds of ceramics are 20 or 30 times faster than that of a carbide material [4]. Therefore, when milling nickel based superalloys, materials with high levels of hardness and high temperature resistance, SiAlON (solid solutions based on the Si3N4 structure) ceramic cutting tools are widely used [3], [5]. However, the plastic flow wear, due to high temperature and high mechanical stress generated in these cutting tools, enhances and propagates cracks, leading eventually to tool failure.

Tool failure in SiAlON ceramic cutting tools can be highly variable, resulting in a very unpredictable tool life. For this reason, it has become relevant to try and monitor the condition of these ceramic tools during the milling process [6]. By continuously measuring the actual wear that these cutting tools develop, it would be possible to prevent either discarding of the tools when they are still usable or, alternatively, over-usage, which could in turn lead to failure and possible damage to the work piece.

Vision sensors can permit, using Digital Image Processing, the continuous and online extraction of information from areas of interest, such as a cutting tool in a machining process [7]. Digital Image Processing refers to the processing of digital images through a computer [8]. This processing is generally done through software that can manipulate the structure of the images and extract relevant information. The relative low cost and high availability of vision sensor devices, such as CCD cameras or SLR cameras, has enabled their use in different aspects of condition monitoring. At present, most tool monitoring vision systems rely on the processing of images of the cutting inserts. In order to obtain these images, the machining program has to be interrupted and the inserts removed from the tool [9]-[12]. This can be a time-consuming process.

Fig. 1 High speed milling process using ceramic cutting tools

The milling of nickel-based alloys with SiAlON cutting tools is generally performed without any coolant, making it a dry machining process. This condition enables the formation of large and very visible sparks emanating from the cutting area as shown in Fig. 1. It is proposed in this work that a relationship exists between the cutting tool wear and the evolution of specific features of the cutting sparks. Using a visual imaging system, it would be possible to monitor the evolution of the cutting sparks through computer vision and image processing techniques; then, this evolution could be

J. A. Dominguez Caballero*, G. A. Manson, and M. B. Marshall are with the Department of Mechanical Engineering, The University of Sheffield, Mappin Street, Sheffield, S1 3JD, UK (*corresponding author, phone: +44(0)7463771039; e-mail: jadominguezcaballero1@sheffield.ac.uk;).

later compared to actual tool wear. Whilst this is an initial approach to the proposed spark-insert wear relationship, the final objective of this research would be to create an online or in-process tool condition monitoring system for an industrial level.

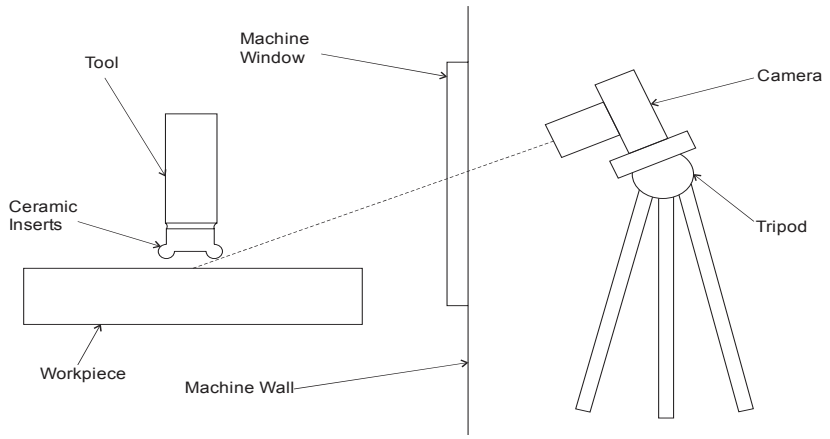

Fig. 2 Camera set-up

II. System Configuration

In Fig. 2, a schematic of the system configuration is shown. A monitoring system was built using a regular SLR Canon EOS 60D digital camera, set to record images of the cutting area of the machining process. The milling machine used was a Starrag ZT 1000 5 axis CNC with a Siemens Sinumerik 840D controller. During machining time, the camera would capture many images at a constant rate, with special focus on the sparks that this process produced. Later, these images were extracted and processed using the software MATLAB[1].

A. Machining

As mentioned previously, the study was performed using a five axis high speed milling machine, and the test used the machining parameters shown in Table I. The cutting tools used were SiAlON ceramic inserts RNGN120400E 6060 from Sandvik Coromant, in a holder of four inserts. Finally, the work piece was a Waspaloy ring and the general standardized composition of this material is shown by Table II.

TABLE I
Machining Cutting Parameters

PARAMETER	VALUE
Cutting Speed Vc (m/min)	875
Feed per minute (mm/min)	1843
Spindle speed n (rev)	4761
Cutting Depth ap (mm)	1.5
Tool Specific Diameter Dc (mm)	50.3
Radial Immersion ae (mm)	29.25
Feed per tooth fz (mm)	0.097
Number of inserts zc	4

B. Image Acquisition

In contrast to the human eye or a video feed, still pictures are a single samples of a short period of time. In an SLR camera, the shutter speed parameter is the one that controls the sample size in a single image. Therefore, the selection of speed parameters can be a common dilemma that is mainly dependent on the application. Through a separate piece of research by the authors of this article in [13], it has been concluded that for the present application, slow imaging settings tend to give better results when processing images from cutting sparks. This is mainly due to the fact that slow imaging settings tend to expand the sample size in still pictures in the time domain. This effect enables the acquisition of a larger amount of spark behaviour data, averaged inside a single image; as opposed to fast settings, that give more instantaneous sets of data, that tend to increase noise when extracting features of spark evolution. The values shown in Table III represent the best combination of parameters when using the slowest shutter speed value, given the environmental illumination conditions. When the shutter speed is the main variable, the values of the diaphragm and ISO can be derived from the said speed. This is the case for the present application, where neither the depth of focus mandated by the Diaphragm, nor the camera sensitivity mandated by the ISO value, are deemed as important as the shutter speed.

III. Area and Intensity Processing

As mentioned previously, the images obtained during the machining process were later extracted and processed. Through a qualitative assessment of the most observable spark features that evolve during the machining process, spark area and spark intensity were selected to be extracted. Other visible features were also assessed, such as spark angle and change in colour, but both of these features would tend to peak or change very early in the first minute of the machining process, and stayed constant for the rest of the sequence.

The processing of the spark area and intensity was done through the generalised algorithm found in Fig. 3. For each feature however, there were different steps and approaches

[1] MATLAB and Image Processing Toolbox Release 2015b, The MathWorks, Inc., Natick, Massachusetts, United States.

inside each of the four algorithm stages.

TABLE II
WASPALOY GENERAL COMPOSITION

ELEMENT	MIN	MAX
Carbon	0.02	0.10
Manganese	--	0.50
Silicon	--	0.75
Chromium	18.0	21.0
Nickel	Balance	
Boron	0.003	0.008
Iron	--	2.00
Cobalt	12.0	15.0
Titanium	2.60	3.25
Aluminium	1.00	1.50
Molybdenum	3.50	5.00
Zirconium	0.02	0.12
Copper	--	0.10
Sulphur	--	0.02

TABLE III
SLOW CAMERA PARAMETERS

PARAMETER	VALUE
Shutter Speed	1/5s
Diaphragm	F22
ISO	5000

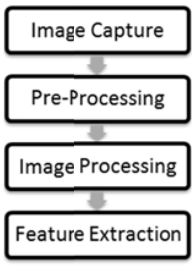

Fig. 3 General algorithm structure for spark area and intensity

A. Area Extraction

In the Pre-Processing stage, the first image of the compound was loaded into the algorithm as a reference image, having almost no spark visible but information about the background layout. This reference image's contrast was then enhanced using a colour adjustment that was used later for the rest of the images and that will be explained later. Then, this reference image was converted into grey scale for further processing.

At the final step of this stage, the rest of the images were loaded into the algorithm. The levels of intensity inside the spark (Fig. 4 (a)) at the red and green channels were very high, while the blue levels where quite low, compared to the rest of the image. A colour adjustment was then applied to the images, as it was done to the reference image. This colour adjustment consisted in taking the values inside a low and high limit for each colour channel of the images, and map these values into the whole intensity range of 0 to 255. Fig. 4 (b) shows the result of the colour adjustment applied to all the images, where only high levels of red, green and blue values were taken and re-mapped. Finally, each image was converted into grey scale individually, as illustrated in Fig. 4 (c).

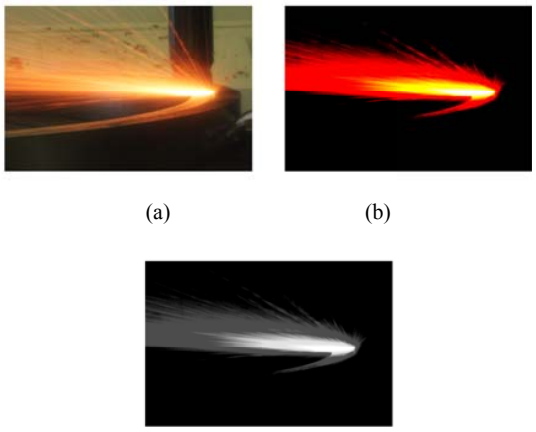

(a) (b)

(c)

Fig. 4 Spark area pre-processing (a) original image, (b) enhanced image, and (c) grey scale image

At the Image Processing stage, the reference image was subtracted from each image, in order to eliminate background information. The resulting image was then converted into binary, where the selection of the binary conversion threshold can be seen in Fig. 5 (b). The value of 0.04 appears to comprise most of the spark core area, without taking much noise from the image as it is the case of lower thresholds, or losing the spark shape, as it can be seen with higher threshold values.

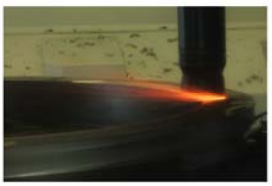

(a)

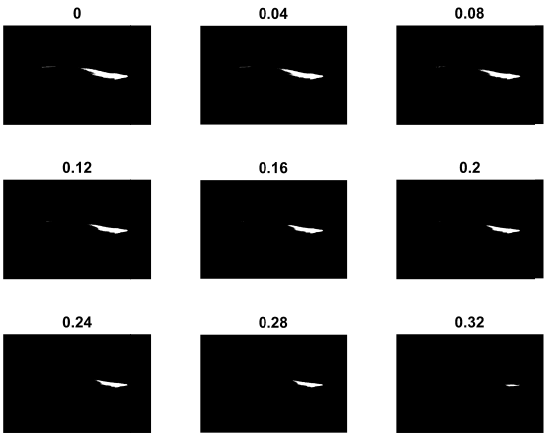

(b)

Fig. 5 Binary conversion (a) original image, and (b) binary conversion threshold selection

After this, it was possible to identify the different connected components of the image and discriminate each component by size, as shown in Fig. 6. At this point, it became possible to quantify the areas of these connected components by the amount of pixels each one contained.

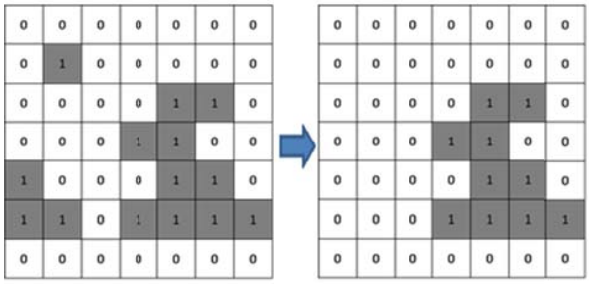

Fig. 6 Connected component discrimination

Given that all the previous steps of the processing algorithm were mainly oriented to the isolation of the spark in each image, it can be concluded that the largest connected component of each image corresponded to the actual spark. Therefore, the final stage of Feature Extraction simply consisted in the extraction of the maximum area.

B. Intensity Extraction

For the extraction of intensity, the initial stage of Image Production has the exact same structure as in the area extraction. Nevertheless, in order to successfully isolate and enhance the spark intensity, a filtering step would be required further ahead in the algorithm. An analysis of different filters and parameters was conducted, and it was concluded that a Low-Pass filter was the most adequate in successfully isolating the spark intensity from the background; therefore, it was important at this point to create a Low-Pass filter mask.

At the Image Processing stage, again the subtraction of the reference image R to each image I_k was carried out for background elimination (1). The resulting image was then filtered in the frequency domain by the Low-Pass mask H previously created, as shown in Fig. 7 (b). The size of this mask was derived from the values in the frequency spectrum, shown in polar form in Fig. 7 (a). The frequency spectrum has a zero frequency value at the center, with frequencies increasing radially; therefore, the mask needed to pass only values of this central area of low frequency, while cutting off high frequencies.

$$Intensity(k) = max\{\sum_{xy}[(I^k - \mathrm{R}) \otimes \mathcal{F}^{-1}(H)]\} \quad (1)$$

With the aid of this filter, the intensity of the spark governed the total intensity of the image as shown in Fig. 7 (c). This made possible to perform a simple summation of the entire image matrix into a single value, as expressed previously in (1), in order to represent the spark intensity of each image at the Feature Extraction stage.

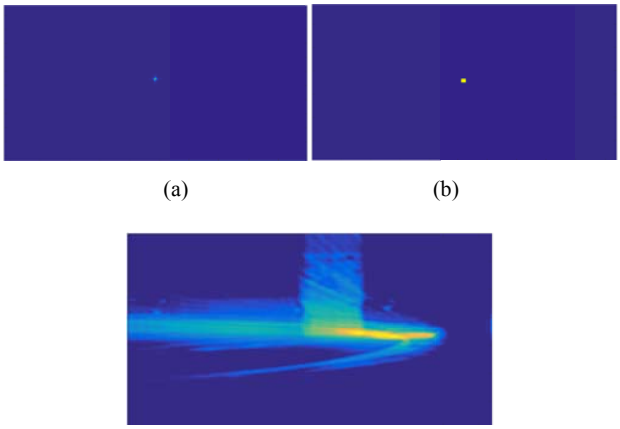

(a) (b) (c)

Fig. 7 Image Processing (a) image in frequency domain, (b) low-pass filter mask, and (c) filtered image

IV. Results

A. Insert Wear Assessment

In order to extract the wear values of the actual ceramic tools, it was necessary to stop the machining process and extract a ceramic insert for inspection. During these breaks in the machining, images of the insert's rake face were recorded. Image processing could also be employed to extract direct wear data from the inserted tools by extracting the area of the inserts worn rake face, also known as crater wear. With a similar procedure as the spark area extraction, the worn surface of the insert could be identified and isolated for the extraction of an area value, as shown in Fig. 8.

(a) (b)

Fig. 8 Ceramic insert's crater wear area extraction with image processing (a) original image, and (b) processed worn area

Fig. 9 shows the increase in the insert's crater wear area throughout the machining time with nine values of wear, counting the initial state where no wear is visible. Also, the area values are given in mm^2, as the size of each pixel was previously calculated. However, the wear trend in Fig. 9 corresponds to a machining process with multiple interruptions for the assessment of the inserts. It may be argued that a different crater wear area trend could have occurred without these interruptions, and that this could have presented lower levels of tool wear. This is due to the ever-present limitation in ceramic materials of brittle fragility where, in general, the continuous impact in milling operations tends to lead to chipping and tool failure [14].

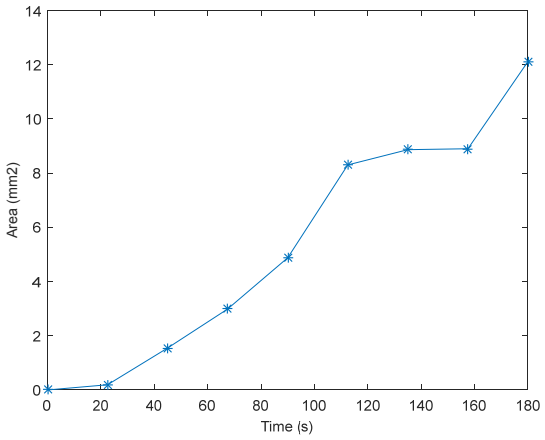

Fig. 9 Insert's crater wear area values

B. Spark Feature Assessment

The spark area and intensity evolution graphs can be seen in Fig. 10, where (a) shows how the total intensity of the spark increases continuously with the machining time, while (b) shows similar behaviour in the spark area evolution. Some specific changes in both features coincide, such as the sudden increase in spark intensity at the time of 60 seconds, as well as the general expected gradual increasing trend, showing that both descriptors are representative of the spark development.

When both descriptors are graphed along with the wear measurements obtained previously (Fig. 10), a similar and consistent general behaviour can be observed in all three measures. This is also shown in Fig. 11. It is possible to see that all three have a general qualitative correlation, as the steepness of the three are very similar; however, it was not possible to quantify this correlation as there is a dimensional mismatch between the number of values of the sparks descriptors and the values of insert wear.

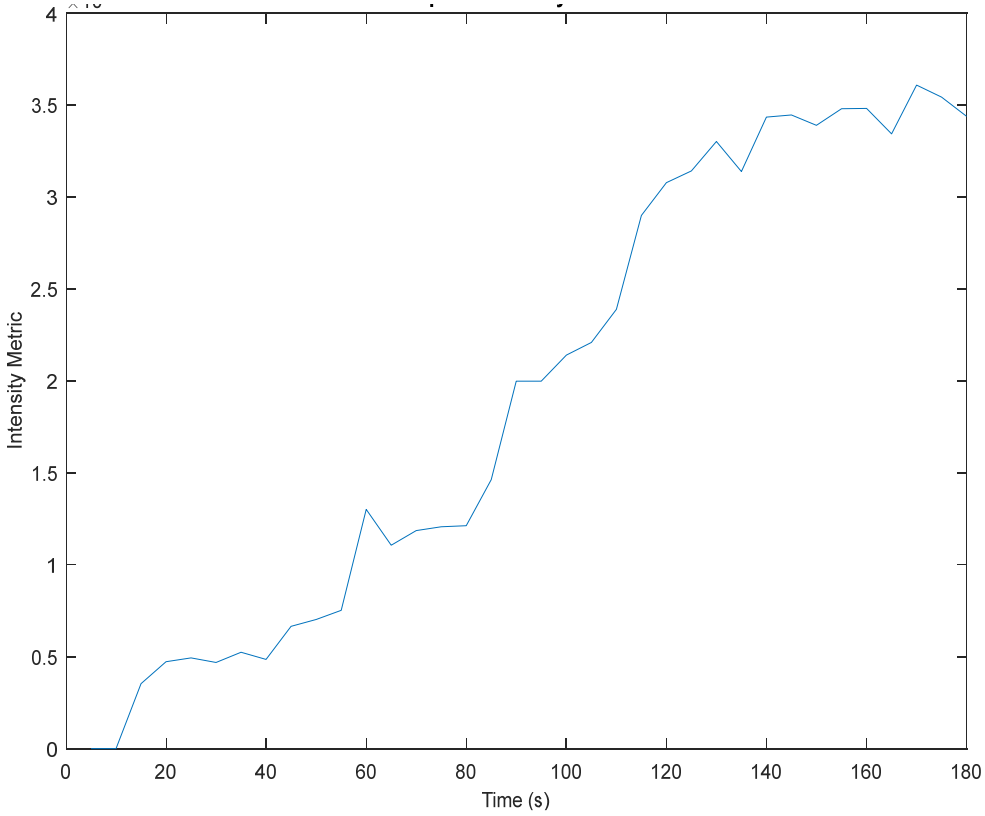

(a)

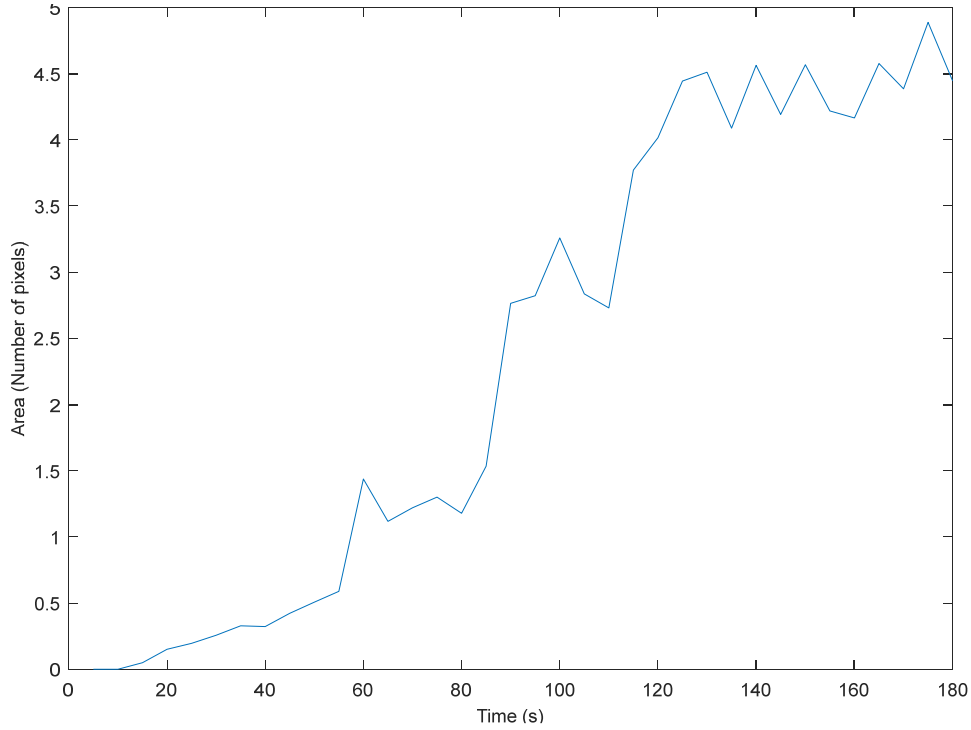

(b)

Fig. 10 Spark evolution (a) intensity, and (b) area

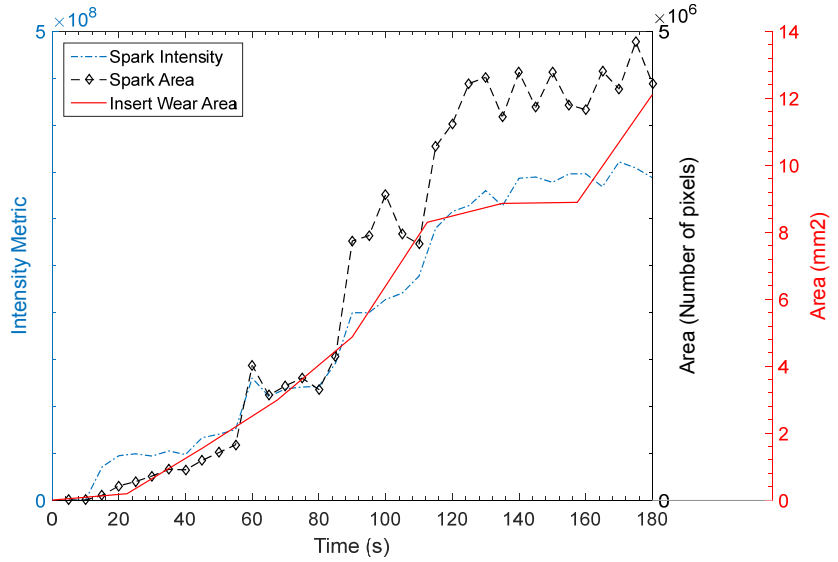

Fig. 11 Spark area, intensity and insert's crater wear area

V. Discussion

While there was some partial discussion with some of the results presented previously, there are other important aspects that shall be outlined. Firstly, algorithms appear to be functioning as intended. There was as expected, a general gradual increase of area and intensity with machining time. For the purpose of tool wear extraction, it becomes apparent in the authors view, that these two features are indeed the most relevant. However, there is still further scope for optimisation of the feature extraction algorithms presented. Also, the general similarity between the spark area, intensity and insert wear shows that there is an evident intrinsic correlation between these, making possible the idea of exploring further tool monitoring systems using this phenomenon. Yet, a more in-depth analysis would be appropriate to understand better the wear mechanisms of the ceramic SiAlON inserts.

Nevertheless, there were several limitations within this initial investigation that could be addressed in future work.

The imaging system, for instance, was quite basic, using an SLR camera with very wide gaps of data between samples, given that the images had a five seconds gap. In this regard, it would be important to find a way to assess which would be the optimal imaging acquiring system, as well as the optimal imaging parameters. As it was mentioned previously in this work, a set of quite "slow" settings were used. It would be interesting; however, to make sure that faster settings are indeed not appropriate for this application. Furthermore, it could be argued that a video feed may be more adequate for further processing rather than still images, as this could provide more information.

The wear assessment technique presented in this work of measuring crater wear area through image processing could be regarded as a basic method of obtaining wear data from the ceramic tools. A more in-depth analysis of other wear mechanisms in SiAlON inserts should be carried out, where perhaps a richer source of wear measurement could be found. Other techniques such as the extraction of weight measurements to find volumetric changes of the cutting tool could show improved results. Or even yet, some measurement of flank wear or notch wear could provide a better tool wear trend [14], [15]. Alternatively, more sophisticated technology, such as 3D imaging through scanners or simple stereo-vision could be beneficial as an in-situ assessing technique. Nevertheless, there would continue to be significantly less wear data than spark data, due to the requirement of stopping machining operation.

There is also future work regarding further analysis of this possible tool monitoring system or technique, as there are many variables associated with this type of metal cutting processes. Machining parameters, such as feed, speed and depth of cut are just a few of the process variables that could give very different results in the way the cutting spark evolves. Also, regarding the image acquisition side of the monitoring system, alternative values for the previously mentioned imaging settings or even external factors like illumination, reflections and camera location, could greatly alter this spark-wear relation.

Even though other techniques of tool wear assessment through visual sensing, such as the ones mentioned at the beginning of this article, appear to give a more precise quantification of tool wear, their limitation of process interruption is inevitable. Yet, the present tool monitoring technique, also through visual sensing, has shown considerable promise for the live assessment of tool wear. Therefore, a fully functional system using this technology could be a highly productive and low costed instrument for high speed machining processes in the manufacturing industry in the near future.

VI. Conclusions

In the machining of nickel-based superalloys, ceramic inserted tools such as SiAlONs are used for their great efficiency regarding high machining speeds. However, these tools can present very unpredictable tool life spans, making a tool monitoring technique or system important for further increase machining efficiency. A relation between the dry cutting process sparks and the actual cutting tool wear was explored and can be summarised through the following conclusions:

- Image processing algorithms for the extraction of cutting spark Intensity and Area can be successfully applied to still images from the machining process.
- These two parameters are good representatives of the cutting spark evolution throughout machining time.
- When the two image processing parameters are compared to the actual cutting tool crater wear area, a qualitative correlation and similarity is evident.
- Further analysis and work is required to explore this relationship further, along with all the different variables that could alter it.

Acknowledgment

The main author would like to thank the Mexican Government Foundation CONACyT for the financial support for this research.

References

[1] Z. Liu, X. Ai, H. Zhang, Z. Wang, and Y. Wan, "Wear patterns and mechanisms of cutting tools in high-speed face milling," in *The 10th International Manufacturing Conf. in China, Journal of Materials Processing Technology*, vol. 129, Fujian, China, 2002, pp. 222-226.

[2] S. Casto, E. Valvo, V. Ruisi, E. Lucchini, and S. Maschio, "Wear mechanism of ceramic tools," in *Wear*, vol. 160, 1993, pp. 227-235.

[3] A. Altin, M. Nalbant, and A. Taskesen, "The effects of cutting speed on tool wear and tool life when machining Inconel 718 with ceramic tools," in *Materials & Design*, vol. 28, 2007, pp. 2518-2522.

[4] Sandvik Coromant, "Ceramics," AB Sandvik Coromant, 2010, Available: http://www.sandvik.coromant.com/sitecollectiondocuments/downloads/global/brochures/en-gb/c-2929-61.pdf.

[5] X. Tian, J. Zhao, J. Zhao, Z. Gong, and Y. Dong, "Effect of cutting speed on cutting forces and wear mechanisms in high-speed face milling of Inconel 718 with Sialon ceramic tools," in *The International Journal of Advanced Manufacturing Technology*, vol. 69, London: Springer, 2013, pp. 2669-2678.

[6] G. Byrne, D. Dornfeld, I. Inasaki, G. Ketteler, W. König, and R. Teti, "Tool Condition Monitoring (TCM) — The Status of Research and Industrial Application," in *CIRP Annals - Manufacturing Technology*, vol. 44, 1995, pp. 541–567.

[7] S. Kurada and C. Bradley, "A machine vision system for tool wear assessment," in *Tribology International*, vol. 30, 1997, pp. 295–304.

[8] R. C. Gonzalez and R. E. Woods, *Digital Image Processing: International Edition*, 3rd ed. New Jersey: Pearson Prentice Hall, 2010, pp. 23.

[9] D.M. D'Addona and R. Teti, "Image Data Processing via Neural Networks for Tool Wear Prediction," in *8th CIRP Conf. on Electro Physical and Chemical Machining (ISEM XVIII)*, vol. 12, 2013, pp. 252–257.

[10] S. Kurada and C. Bradley, "A review of machine vision sensors for tool condition monitoring," in *Computers in Industry*, vol. 34, 1997, pp. 55-72.

[11] T. Pfeifer and L. Wiegers, "Reliable tool wear monitoring by optimized image and illumination control in machine vision," in *Measurement*, vol. 28, 2000, pp. 209-218.

[12] T. Teshima, T. Shibasaka, M. Takuma, A. Yamamoto, and K. Iwata "Estimation of Cutting Tool Life by Processing Tool Image Data with Neural Network," in *CIRP Annals - Manufacturing Technology*, vol. 42, 1993, pp. 59-62.

[13] J. A. Dominguez Caballero, G. A. Manson, and M. B. Marshall, "Optimal image processing acquisition parameters for a tool condition monitoring system of ceramic inserted tools," unpublished.
[14] JP. Davim, *Machining of Hard Materials*, New York: Springer Science & Business Media, 2011, pp. 38.
[15] W. Grzesik, *Advanced Machining Processes of Metallic Materials: Theory, Modelling and Applications*, Elsevier, 2008, pp. 163-166.